Supplementary Materials

Engineering hollow porous carbon confined Ru-MgO hetero-structured nanopair as high-performance catalyst for ammonia borane hydrolysis

Jialei Yang[a, #], Zhenyu Yang[b, #], Jiafu Li[a], Hao Gang[a], Donghai Mei[c], Dongming Yin[d], Ruiping Deng[d], Yifeng Zhu[e], Xingyun Li[a,*], Ning Wang [a,*], Sameh M. Osman[f], Yusuke Yamauchi[g,h,i]

[a]Institute of Materials for Energy and Environment, College of Materials Science and Engineering, College of Chemistry and Chemical Engineering, Qingdao University, Qingdao 266071, China

[b]College of Electronics and Information, Qingdao University, Qingdao 266071, China

[c]Tianjin Key Laboratory of Green Chemical Engineering Process Engineering, Tiangong University, Tianjin 300387, China

[d]State Key Laboratory of Rare Earth Resources Utilization, Changchun Institute of Applied Chemistry, Chinese Academy of Sciences, Changchun 130022, China

[e]Shanghai Key Laboratory of Molecular Catalysis and Innovative Materials, Fudan University, Shanghai 200433, P. R. China

[f]Chemistry Department, College of Science, King Saud University, P.O. Box 2455, Riyadh 11451, Saudi Arabia

[g]Department of Materials Process Engineering, Graduate School of Engineering, Nagoya University, 464-8603 Nagoya, Japan

[h]Department of Chemical and Biomolecular Engineering, Yonsei University, 50 Yonsei-ro, Seodaemun-gu, Seoul 03722, South Korea

[i]Australian Institute for Bioengineering and Nanotechnology (AIBN), The University of Queensland, Brisbane, QLD 4072, Australia

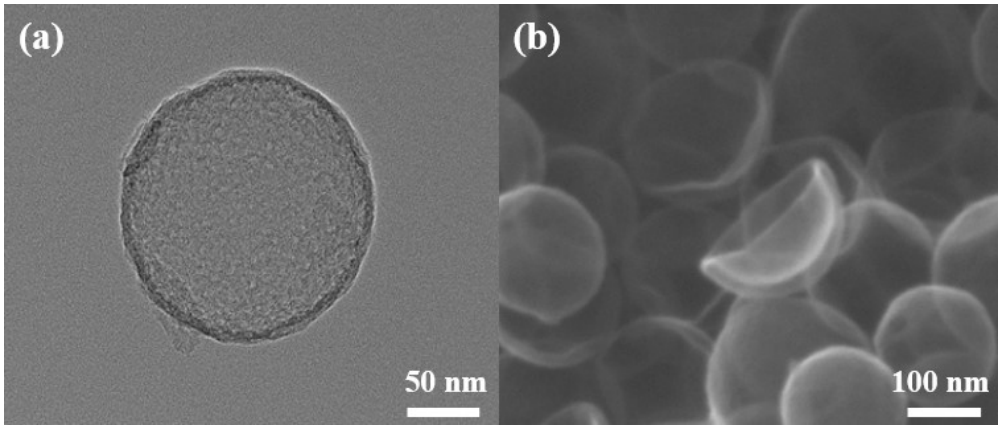

Fig. S1. (a) TEM and (b) SEM images of HBC.

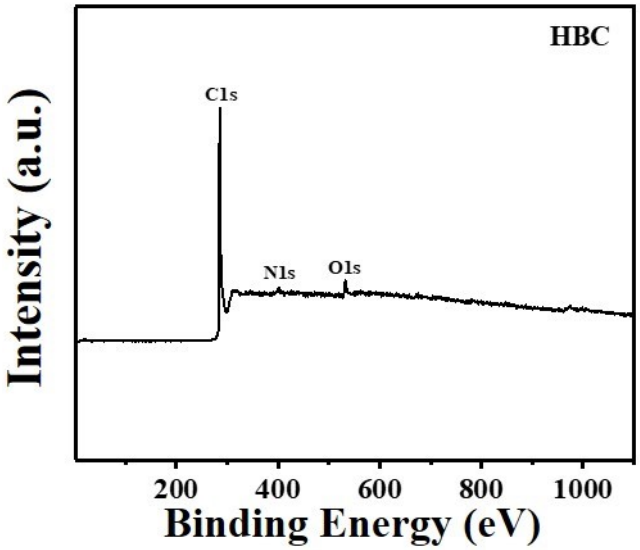

Fig. S2. XPS curve of HBC.

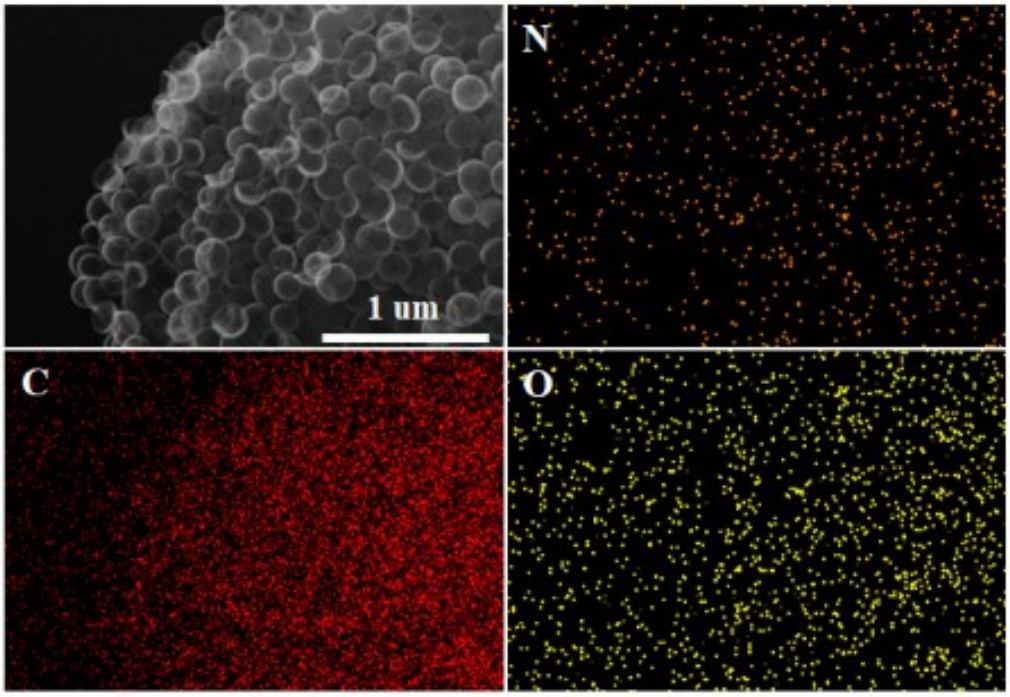

Fig. S3. SEM image and EDS elemental mappings of N, C, O respectively for HBC.

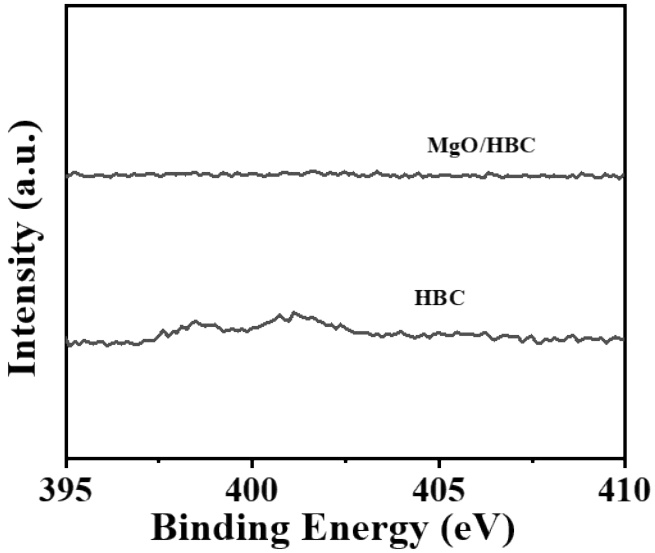

Fig. S4. Deconvolution of N 1s XPS spectra for HBC and MgO/HBC.

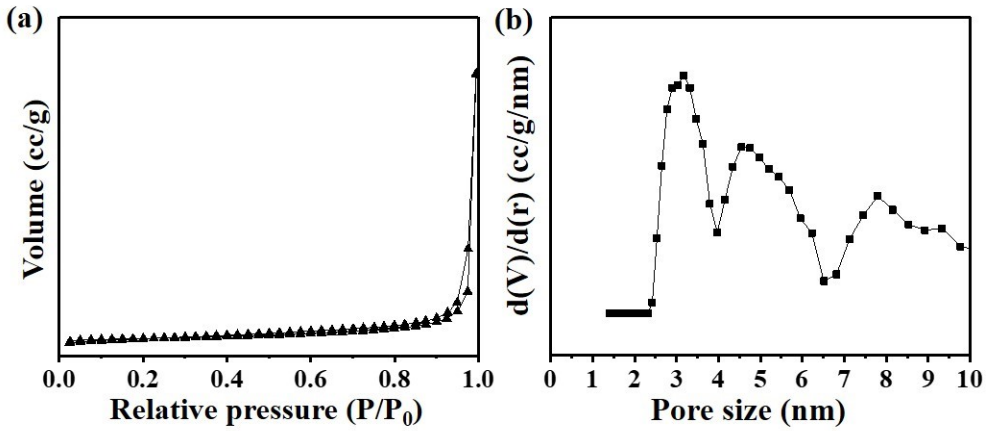

Fig. S5. (a) N_2 adsorption-desorption isotherms, (b) NL-DFT pore size distribution of MgO.

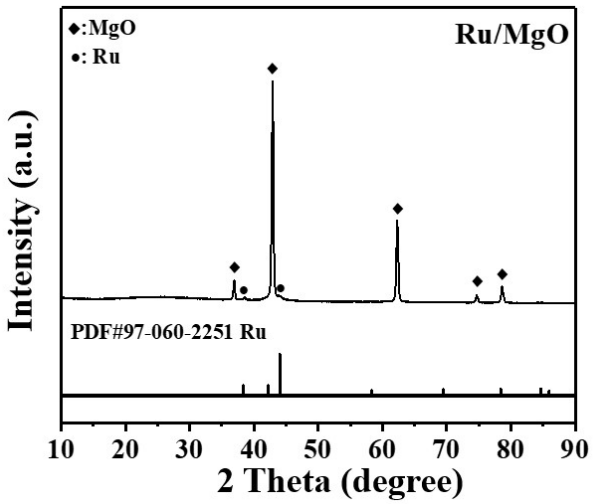

Fig. S6. XRD pattern of Ru/MgO.

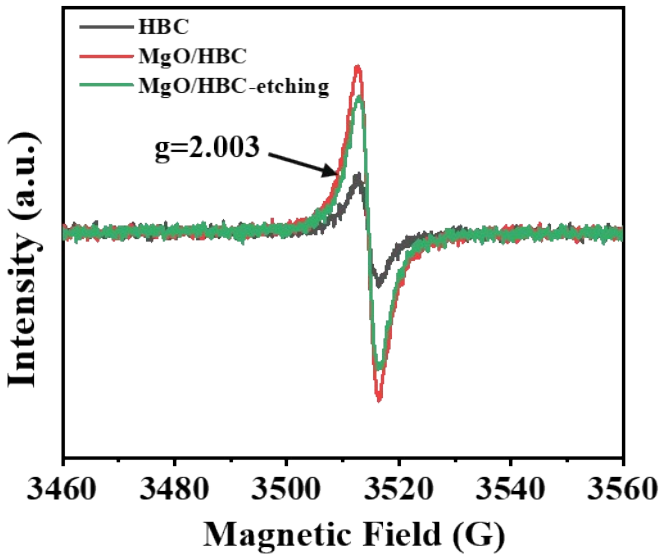

Fig. S7. EPR curves of HBC, MgO/HBC and MgO/HBC-etching.

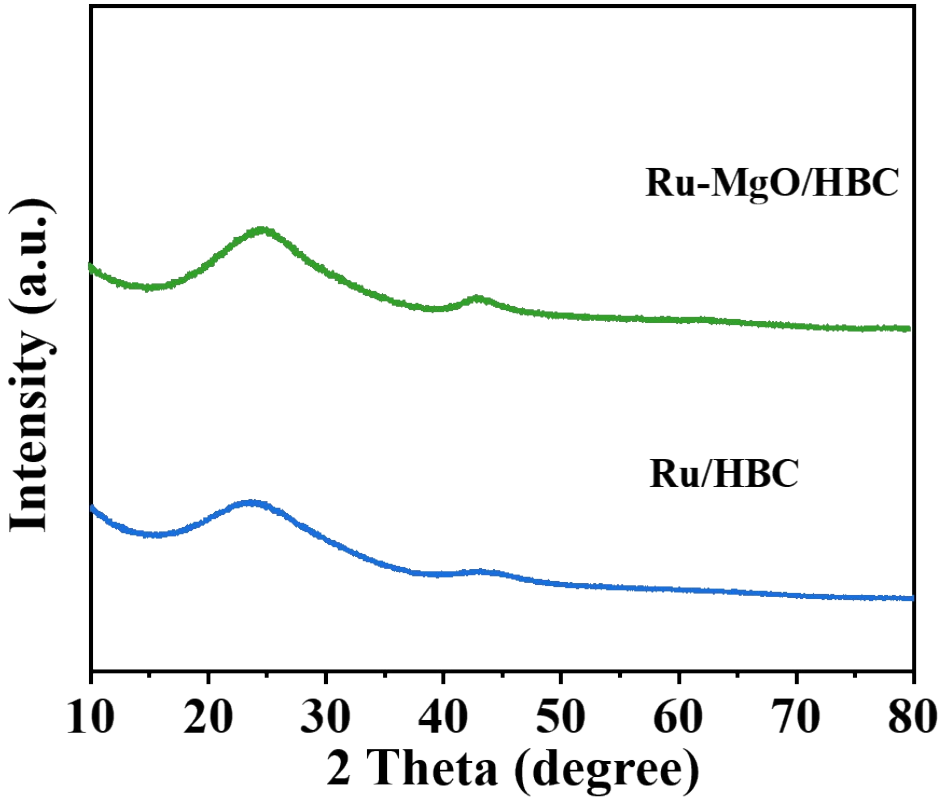

Fig. S8. XRD patterns of Ru/HBC and Ru-MgO/HBC.

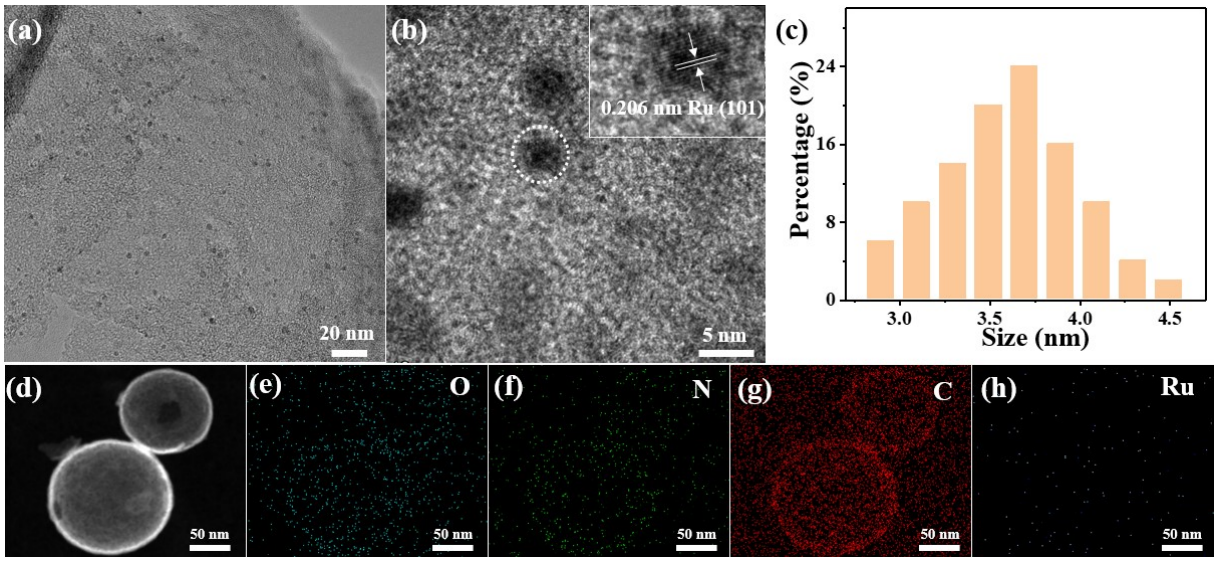

Fig. S9. (a) TEM image, (b) HR-TEM image (inset is the enlargement of Ru nanoparticle), (c) size distributions of Ru catalyst, (d) STEM, (e-h) EDS elemental mapping images of O, N, C, Ru respectively for Ru/HBC.

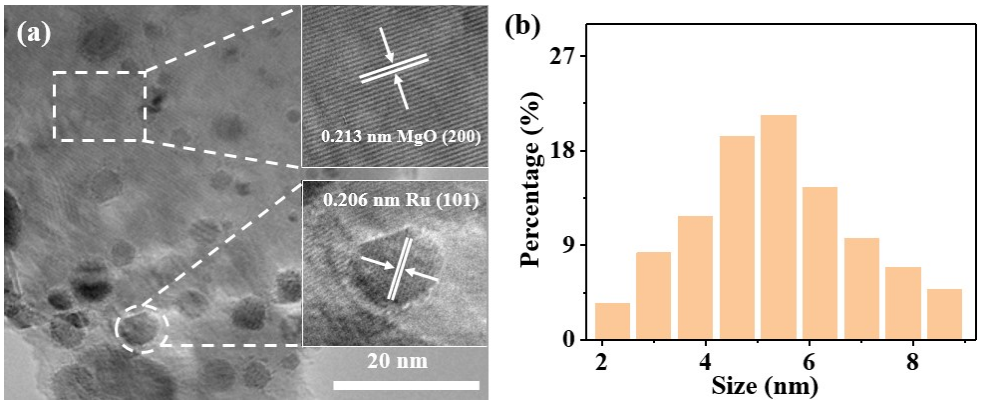

Fig. S10. (a) TEM images, (b) size distributions of Ru nanoparticles of Ru/MgO.

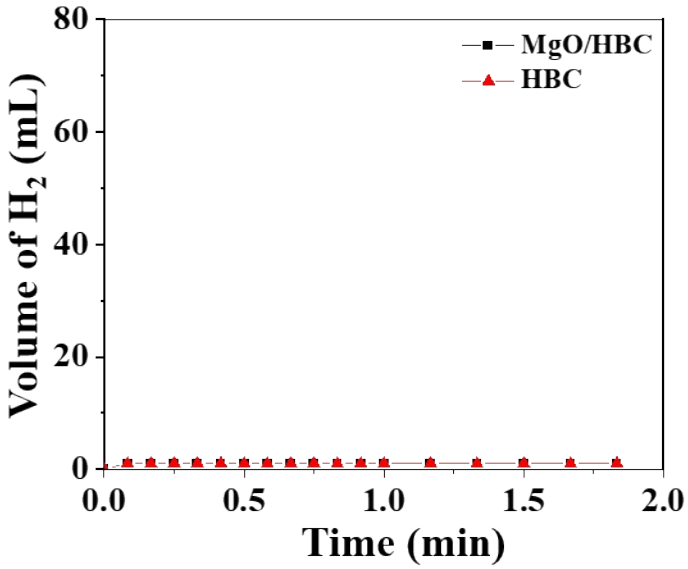

Fig. S11. Volume of the H_2 generated from AB hydrolysis versus time at 298 K catalyzed by HBC and MgO/HBC.

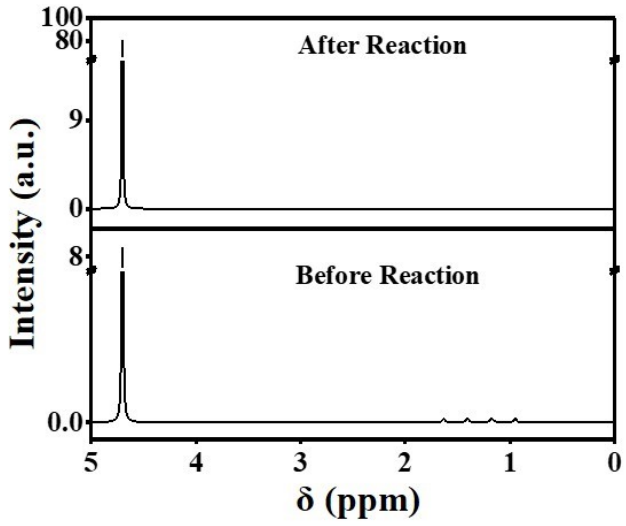

Fig. S12. ^1H NMR spectra of the NH_3BH_3 solution before and after reactions.

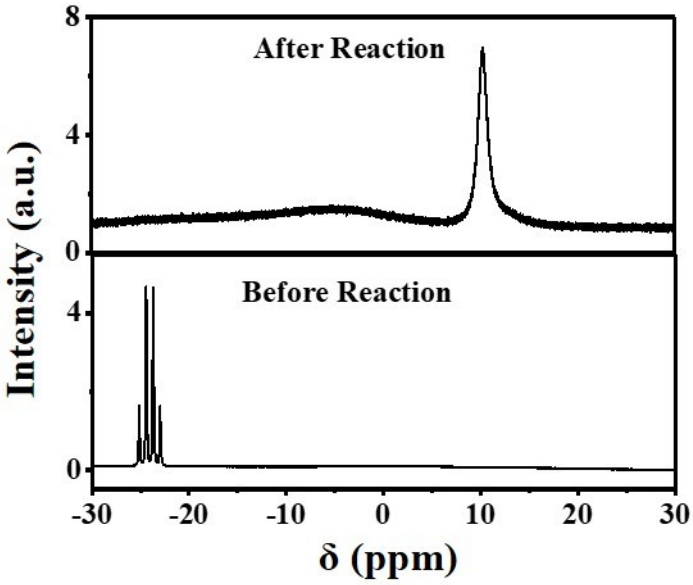

Fig. S13. ^{11}B NMR spectra of the NH_3BH_3 solution before and after reactions.

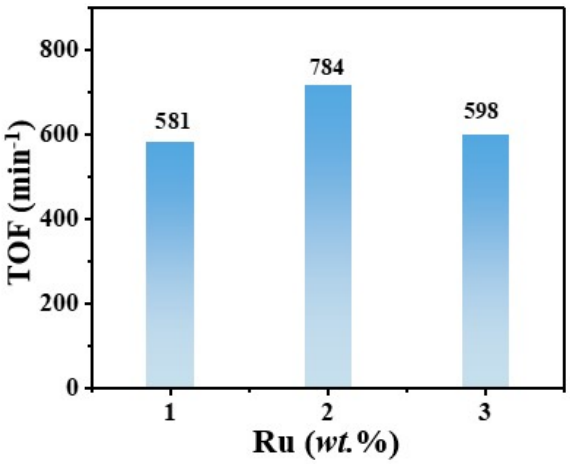

Fig. S14. TOF value for Ru-MgO/HBC at various Ru loading.

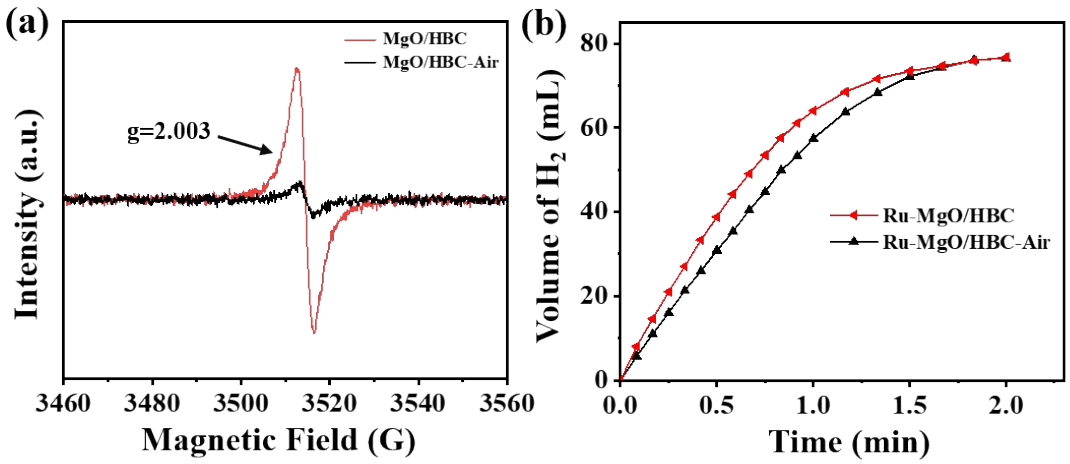

Fig. S15. (a) EPR spectra, (b) volume of the H_2 generated from AB hydrolysis versus time at 298 K over catalysts of Ru-MgO/HBC and Ru-MgO/HBC-Air.

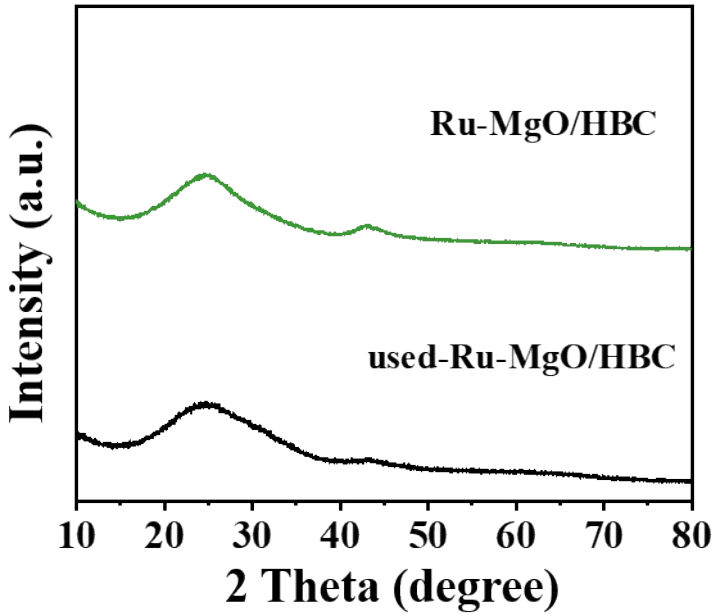

Fig. S16. XRD pattern of Ru-MgO/HBC and used-Ru-MgO/HBC.

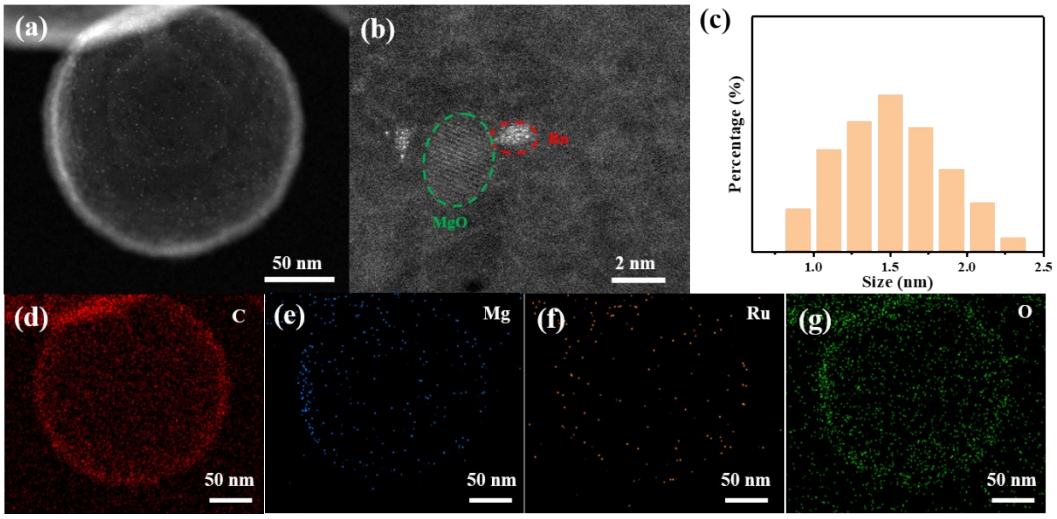

Fig. S17. (a) TEM images, (b) size distributions of Ru nanoparticles of used-Ru-MgO/HBC.

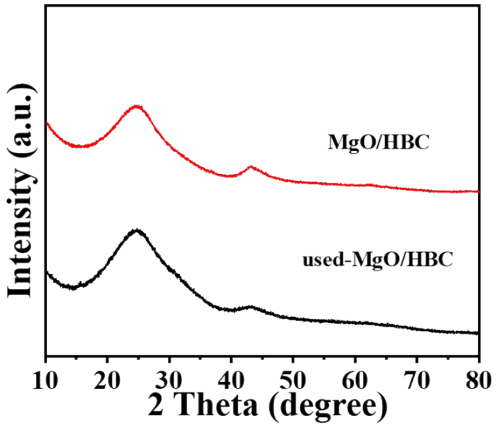

Fig. S18. XRD pattern of MgO/HBC and used-MgO/HBC.

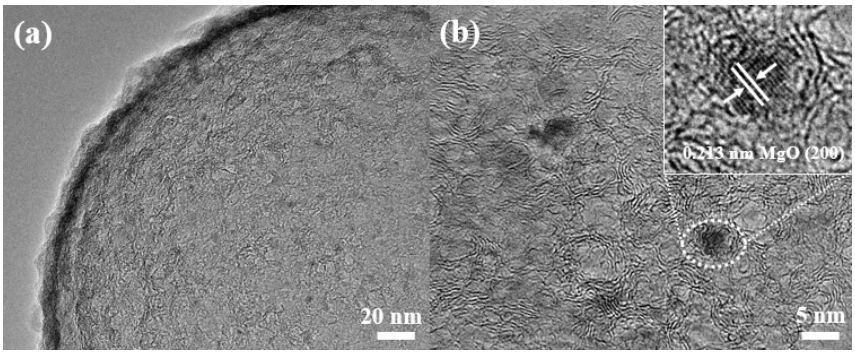

Fig. S19. (a)TEM and (b) HR-TEM images of used-MgO/HBC

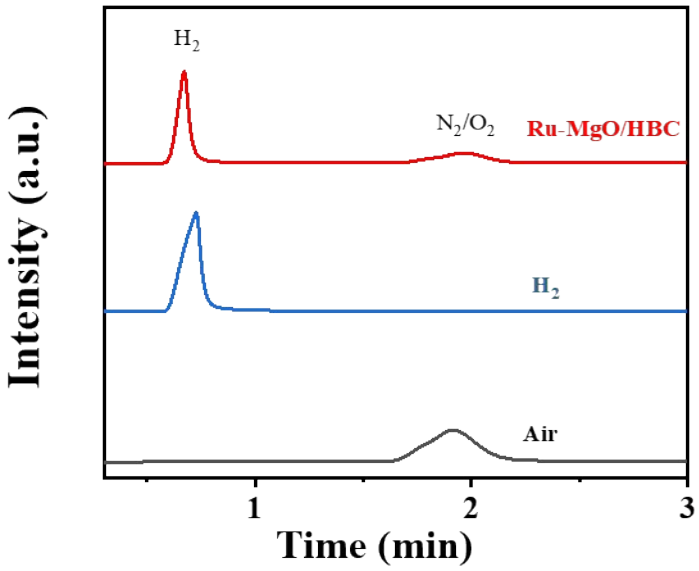

Fig. S20. GC spectra for the released gas from AB hydrolysis over Ru-MgO/HBC, pure H_2 and air.

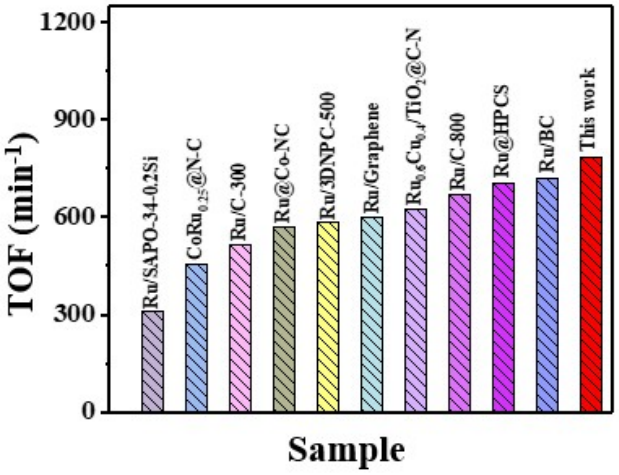

Fig. S21. Catalytic performance of various catalysts in aqueous solution as reported in the literature[1-10].

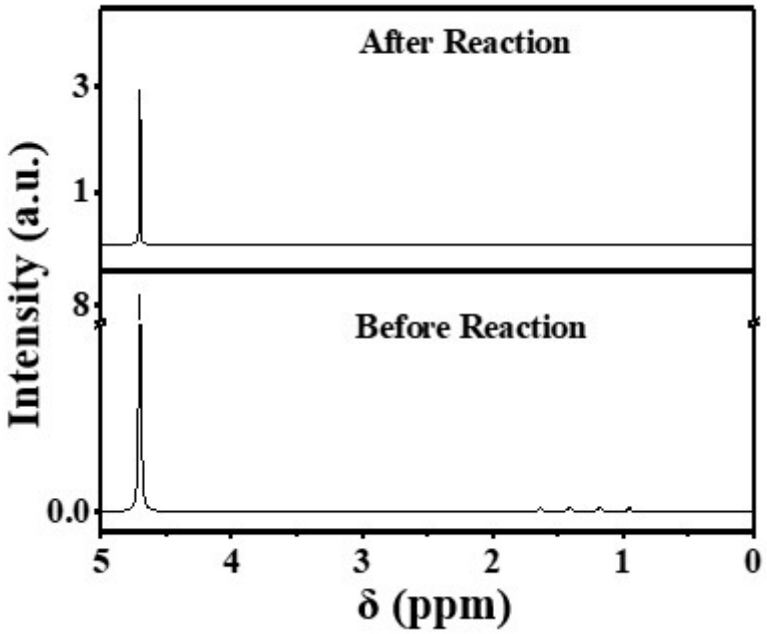

Fig. S22. ^{1}H NMR spectra of the NH_3BH_3 solution before and after reactions in basic solution.

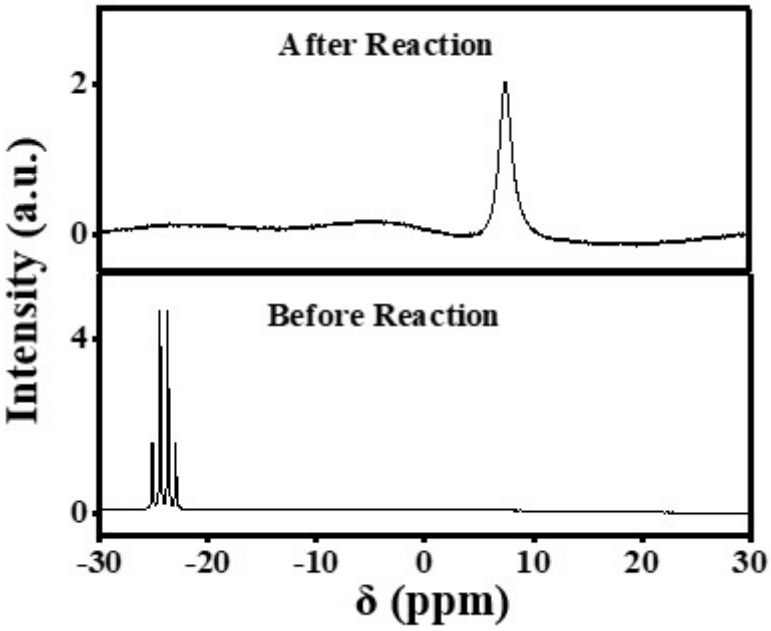

Fig. S23. ^{11}B NMR spectra of the NH_3BH_3 solution before and after reactions in basic solution.

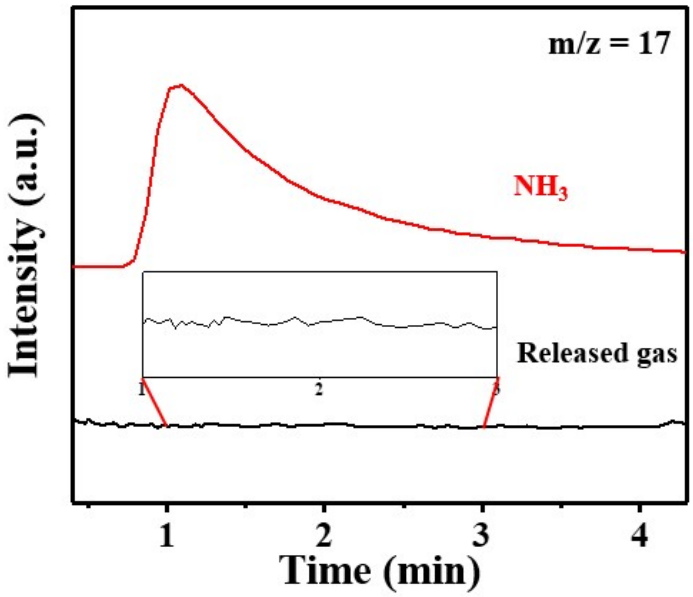

Fig. S24. NH_3 MS signal of the collected gas from AB hydrolysis in alkaline solution and the pure NH_3 reference gas.

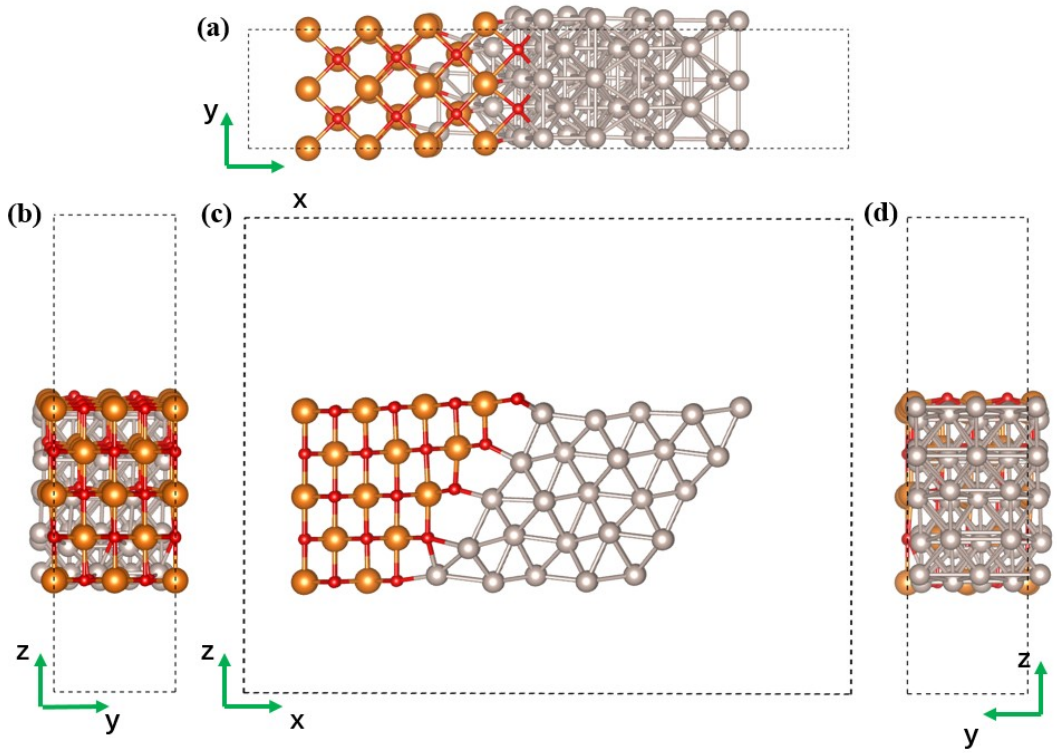

Fig. S25. Front, side and top view of MgO-Ru, grey: Ru, orange: Mg, red: O. The original Ru (101) supercell has a parameter of a=10.129848 A, b=5.4116 A and c (vacuum layer direction) =23.564892 A, while the MgO (200) has a parameter of a=5.955536 A, b=5.955536 A and c (vacuum layer direction) =23.4224 A. The lattice constant of MgO (200) in the b direction is

2.97 in comparison to that of 2.72 for the lattice constant of Ru (101) in the b direction. A 1×2×1 supercell of MgO (200) and Ru (101) was chosen to build the Ru(101)/MgO(200) heterojunctions, and the lattice mismatch between the Ru(101)/MgO(200) heterojunctions is less than 10%.

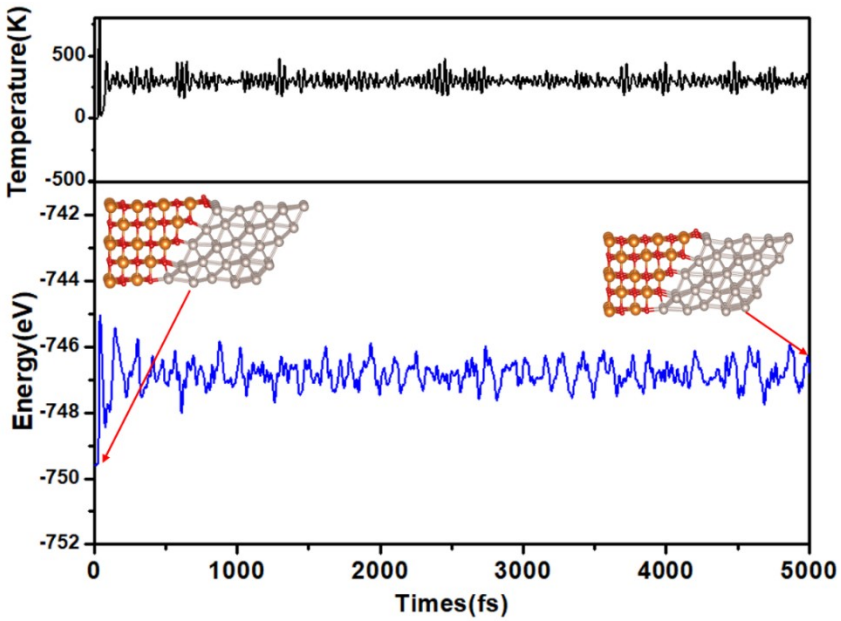

Fig. S26. Variations of energy and temperature versus the AIMD simulation time for MgO-Ru. The insets denote the model of MgO-Ru at the first and last step of AIMD simulation at T = 298 K with a time step of 1 fs. Grey: Ru, orange: Mg, red: O.

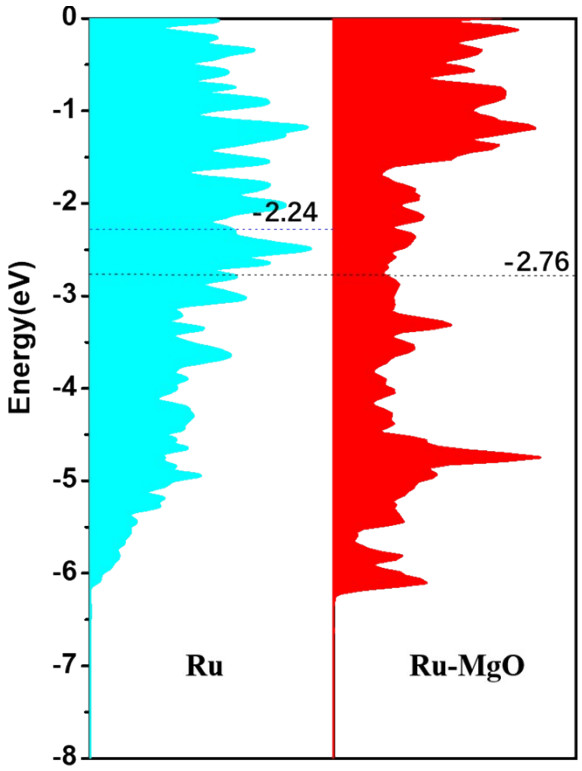

Fig. S27. *d*-band center of Ru and Ru-MgO. The d-band center is calculated by the following equation[11]: $\varepsilon_d = \frac{\int_{-20}^{0} n_d(\varepsilon) * \varepsilon d\varepsilon}{\int_{-20}^{0} n_d(\varepsilon) d\varepsilon}$, wherein ε_d, $n_d(\varepsilon)$ and ε refer to the d-band center, electron density and electron energy with respect to the Fermi level, respectively. The reason why choosing -20 eV as the lower limit is due to that there is no energy lever distribution under this vaule.

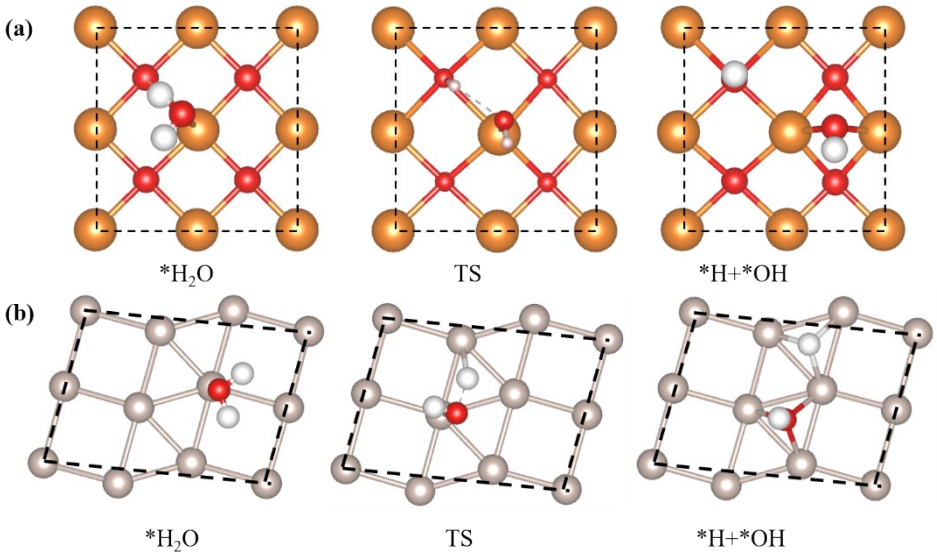

Fig. S28. Optimized structures of the intermediates and transition states at (a) MgO and (b) Ru. grey: Ru, orange: Mg, red: O, white: H.

Table S1. Pore structures and surface information of the catalysts.

Samples	Specific surface area (m^2/g)	Pore volume (cc/g)	Elemental content (*at.*%)		
			C	N	O
HBC	678.6	10.7	94.8	2.4	2.8
MgO/HBC	377.9	6.6	92.3	0.3	7.4
Ru/HBC	631.3	7.6	94.1	2.1	3.8
Ru-MgO/HBC	251.1	3.9	95.2	0	4.8

Table S2. ICP information

Samples	Ru (*wt.*%)	Mg (*wt.*%)
MgO/HBC	-	2.7
Ru/HBC	2.4	-
Ru-MgO/HBC	2.2	2.5

References

1. H. Chu, N. Li, X. Qiu, Y. Wang, S. Qiu, J.-L. Zeng, Y. Zou, F. Xu and L. Sun, *Int. J. Hydrogen Energy*, 2019, **44**, 29255-29262.
2. C. Du, Q. Ao, N. Cao, L. Yang, W. Luo and G. Cheng, *Int. J. Hydrogen Energy*, 2015, **40**, 6180-6187.
3. X. Huang, Y. Liu, H. Wen, R. Shen, S. Mehdi, X. Wu, E. Liang, X. Guo and B. Li, *App. Catal. B, Environ.*, 2021, **287**, 119960.
4. Y. Liu, X. Yong, Z. Liu, Z. Chen, Z. Kang and S. Lu, *Adv. Sustain. Syst.*, 2019, **3**, 1800161.
5. M. Navlani-García, K. Mori, A. Nozaki, Y. Kuwahara and H. Yamashita, *App. Catal. A, Gen.*, 2016, **527**, 45-52.
6. Q. Sun, N. Wang, R. Bai, Y. Hui, T. Zhang, D. A. Do, P. Zhang, L. Song, S. Miao and J. Yu, *Adv. Sci.*, 2019, **6**, 1802350.
7. H. Wang, C. Xu, Q. Chen, M. Ming, Y. Wang, T. Sun, Y. Zhang, D. Gao, J. Bi and G. Fan, *ACS Sustain. Chem. Eng.*, 2019, **7**, 1178-1184.
8. Z. Wei, Y. Liu, Z. Peng, H. Song, Z. Liu, B. Liu, B. Li, B. Yang and S. Lu, *ACS Sustain. Chem. Eng.*, 2019, **7**, 7014-7023.
9. C. Xu, M. Ming, Q. Wang, C. Yang, G. Fan, Y. Wang, D. Gao, J. Bi and Y. Zhang, *J. Mater. Chem. A*, 2018, **6**, 14380-14386.
10. M. Ye, J. Wu and G. Fan, *Fuel*, 2022, **321**, 123982.
11. F. S. Jens K. Norskov, Frank Abild-Pedersen, Thomas Bligaard, *Fundamental Concepts in Heterogeneous Catalysis*, 2014, 114-137.